

Ensembling Diffusion Models via Adaptive Feature Aggregation

Cong Wang^{1†‡}, Kuan Tian^{2‡}, Yonghang Guan², Jun Zhang^{2§}, Zhiwei Jiang^{1§},
Fei Shen², Xiao Han², Qing Gu¹, and Wei Yang²

¹ Nanjing University

`cw@smail.nju.edu.cn`, `{jzw,guq}@nju.edu.cn`

² Tencent AI Lab

`{kuantian,yohnguan,junejzhang,ffeishen,haroldhan,willyang}@tencent.com`

Abstract. The success of the text-guided diffusion model has inspired the development and release of numerous powerful diffusion models within the open-source community. These models are typically fine-tuned on various expert datasets, showcasing diverse denoising capabilities. Leveraging multiple high-quality models to produce stronger generation ability is valuable, but has not been extensively studied. Existing methods primarily adopt parameter merging strategies to produce a new static model. However, they overlook the fact that the divergent denoising capabilities of the models may dynamically change across different states, such as when experiencing different prompts, initial noises, denoising steps, and spatial locations. In this paper, we propose a novel ensembling method, Adaptive Feature Aggregation (AFA), which dynamically adjusts the contributions of multiple models at the feature level according to various states (i.e., prompts, initial noises, denoising steps, and spatial locations), thereby keeping the advantages of multiple diffusion models, while suppressing their disadvantages. Specifically, we design a lightweight Spatial-Aware Block-Wise (SABW) feature aggregator that adaptive aggregates the block-wise intermediate features from multiple U-Net denoisers into a unified one. The core idea lies in dynamically producing an individual attention map for each model’s features by comprehensively considering various states. It is worth noting that only SABW is trainable with about 50 million parameters, while other models are frozen. Both the quantitative and qualitative experiments demonstrate the effectiveness of our proposed Adaptive Feature Aggregation method. The code is available at <https://github.com/tenvence/afa/>.

Keywords: Image Generation · Diffusion Models · Model Ensembling

1 Introduction

Diffusion models [17, 50] have progressively become the mainstream models for text-guided image generation [5, 10, 35, 39, 46, 48, 62], which treats generation as

[†] Work done during an internship at Tencent AI Lab.

[‡] Equal contribution.

[§] Corresponding authors.

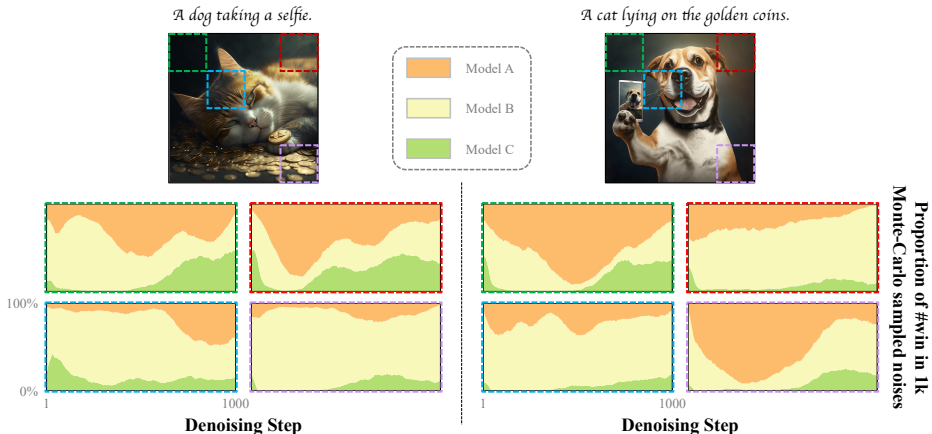


Fig. 1: Examples to illustrate the dynamical change of the denoising capabilities across various states. We conduct experiments on different prompts with various initial noises. We then plot the proportion of *wins* (*i.e.*, the model with the least error between the predicted noise and the initial noise), for each model in a certain spatial region.

an iterative denoising task. Recently, the open-source stable diffusion (SD) [46] model has prompted the development and release of numerous powerful diffusion models within the open-source community (*e.g.*, CivitAI³). These models are typically fine-tuned on various expert datasets, showcasing diverse denoising capabilities. Leveraging multiple high-quality models to dig out better generations is an important research direction, which has not been extensively studied.

Existing methods leverage multiple diffusion models through the weighted merging of model parameters, which can be called the static method. The weights are usually manually set [33, 56] or automatically searched through enumeration [4]. In contrast, model ensembling, which can be called the dynamic method, often uses dynamic strategies to fuse multiple models at the feature level. Unlike ensembling for classification models [12] that usually work after the output, ensembling for diffusion models typically needs to work for each block. However, the denoising capabilities of models vary not only at different blocks but also at different spatial locations. As illustrated in Fig. 1, we conduct denoising experiments on different prompts with various initial noises. Then, we plot the proportion of *wins* (*i.e.*, the model with the least error between the predicted noise and the initial noise), for each model in a certain spatial region, to distinguish the denoising capabilities of the models at different states. In other words, different prompts, initial noises, denoising steps, and spatial locations can all have a significant impact on the denoising capabilities of diffusion models. This implies that an adaptive method is needed to ensure that each diffusion model can dominate the generation at its strongest states.

³ <https://civitai.com/>

In this paper, we propose a novel Adaptive Feature Aggregation (AFA) method, which dynamically adjusts the contributions of multiple models at the feature level by taking into account various states, such as prompts, initial noises, denoising steps, and spatial locations. Specifically, we design a lightweight Spatial-Aware Block-Wise (SABW) feature aggregator that adaptively aggregates the block-level intermediate features from multiple U-Net denoisers into a unified one. The core idea of adaptive aggregation lies in dynamically producing an individual attention map for each model’s features by comprehensively taking into account the various states such as text prompts, denoising steps, and spatial locations. A noteworthy aspect of AFA is that only SABW is trainable with about 50 million parameters, while all other models are frozen.

Our main contributions are summarized as follows:

- We propose an ensembling-based AFA method to dynamically adjust the contributions of multiple models at the feature level.
- We design the SABW feature aggregator that can produce attention maps according to various states to adaptively aggregate the block-level intermediate features from multiple U-Net denoisers.
- We conduct both quantitative and qualitative experiments, demonstrating that our AFA outperforms the base models and the baseline methods in both superior quality and context alignment.

2 Related Work

Text-Guided Image Synthesis. Early works for text-guided image synthesis leverage Generative Adversarial Networks (GAN) [14] conditioned on text [53, 61, 65, 71]. Based on the success of Transformers [54], many subsequent works re-frame text-guided image synthesis as a sequence-to-sequence task [7, 13, 40, 64, 66]. Recently, diffusion models [17, 50] gradually become mainstream, which treats image generation as an iterative denoising task. By injecting text as a condition into the denoising process, many diffusion-based models achieve significant success in text-guided image synthesis [5, 10, 35, 39, 46, 48, 62]. Among them, the Latent Diffusion Model (LDM) [46] performs the diffusion and reverse process in the latent space, instead of the pixel space, which largely reduces the computational burden. Among all the implementations of the Latent Diffusion Model, the stable diffusion model (SD) is the most famous one. Along with its public availability, the open-source community achieves tremendous success, with the emergence of many excellent fine-tuned models. These high-quality models are typically fine-tuned on various expert datasets, showcasing diverse denoising capabilities. In this paper, we aim to leverage multiple such models to achieve stronger text-to-image generation.

Model Merging. For vision or language understanding tasks, the effectiveness of parameter merging [8, 11, 20, 21, 25, 32, 58] can be interpreted from the perspectives of loss landscape [3, 52, 57] and task arithmetic [19, 36, 67]. However,

merging-based methods have not been widely studied for generation tasks, especially diffusion-based generation. Recently, many intuitive merging-based methods have emerged. One of the popular methods is Weighted Merging [56], which manually determines weights to merge each U-Net [47] parameter of multiple SD models. Although the simplicity, Weighted Merging coarsely allocates weight to all U-Net blocks. As an improvement, Merge Block Weighted (MBW) [33] allows for manually setting different merging weights for the parameters of distinct U-Net blocks, which provides a more fine-grained merging strategy. Furthermore, to reduce the reliance on manual weights, autoMBW [4] attempts to automate the merging process, which enumeratively selects the optimal combination of MBW weights by an aesthetic classifier. However, autoMBW is constrained by the performance bottleneck of the aesthetic classifier, and the enumerative selection leads to a huge time consumption to find the optimal settings. Such merging methods can be called the static methods. In this paper, we aim to leverage multiple diffusion models by the dynamic methods, *i.e.*, ensembling.

Model Ensembling. Model ensembling is an effective method to achieve better performance [70], which has been widely applied in various vision understanding tasks, such as classification [45, 63, 69], regression [34, 43], clustering [55]. While fewer works focus on the ensembling of generative models, because of the complexity of image space. Vision-Aided GAN [24] focuses on GANs [14], which guides the optimization of a target generator by ensembling pretrained models as a loss. MagicFusion [68] focuses on the diffusion models, which fuses the predicted noises of two expert U-Net denoisers to implement specific applications, such as style transferring and object binding. In this paper, we aim to efficiently ensemble multiple diffusion models to achieve generation improvements.

3 Method

3.1 Preliminary

As a type of generative model, the diffusion model [17, 50] consists of two processes, which are the diffusion process and the reverse process, respectively. In the diffusion process (*i.e.*, the forward process), the Gaussian noises are iteratively added to degrade the images over T steps until the images become completely random noise. In the reverse process, a trained denoiser is used to iteratively generate images from the sampled Gaussian noise.

When training, given an input image \mathbf{x}_0 and the additional condition \mathbf{c} (*e.g.*, encoded textual prompts *etc.*), the denoising loss is defined as

$$\mathcal{L}_{\text{denoise}} = \mathbb{E}_{\mathbf{x}_0, \epsilon \sim \mathcal{N}(\mathbf{0}, \mathbf{I}), \mathbf{c}, t} \|\epsilon_{\theta}(\mathbf{x}_t, \mathbf{c}, t) - \epsilon\|^2. \quad (1)$$

Among them, $\mathbf{x}_t = \sqrt{\alpha_t}\mathbf{x}_0 + \sqrt{1 - \alpha_t}\epsilon$ is the noisy image at timestep $t \in [1, T]$, where α_t is a predefined scalar from the noise scheduler. ϵ is the added noise. ϵ_{θ} is the denoiser with the learnable parameters θ , which predicts the noise to be removed from the noisy image.

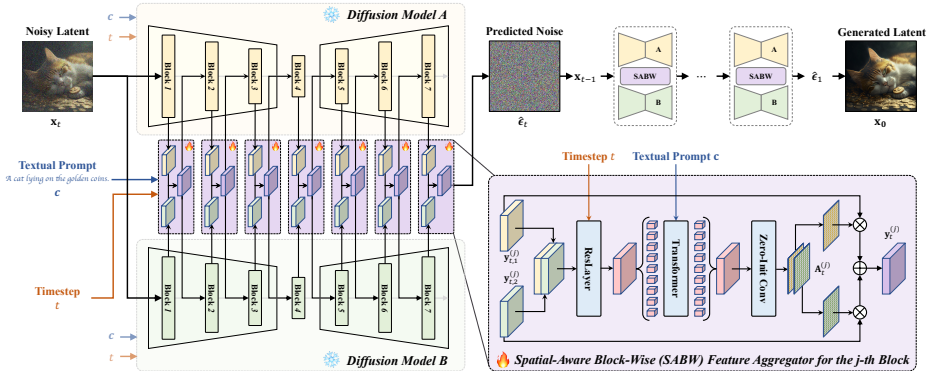


Fig. 2: Framework of ensembling multiple diffusion models by our Adaptive Feature Aggregation (AFA) method.

LDM stands out as one of the most popular diffusion models. It performs the diffusion and reverse process in the latent space which is encoded by a Variational Auto-Encoder (VAE) [22, 44]. In LDM, the U-Net structure [47] is used for denoiser, which contains three parts of blocks, which are the down-sampling blocks, the middle block, and the up-sampling blocks, respectively. Each down-sampling block is skip-connected with a corresponding up-sampling block. These blocks are composed of Transformer [54] layers and ResNet [15] layers. In the Transformer layers, the cross-attention mechanism is employed to incorporate conditional textual prompts, which plays a crucial role in text-guided image generation.

3.2 Adaptive Feature Aggregation

Our proposed Adaptive Feature Aggregation (AFA) ensembles multiple diffusion models that share the same architecture but different parameters. Specifically, SABW is designed to integrate intermediate features from multiple U-Net denoisers at the block level. Fig. 2 demonstrates an example of ensembling two diffusion models, and each U-Net denoiser contains seven blocks by SABW. The forward process of AFA can be seen in Algorithm 1.

Given N diffusion models to be ensembled, whose U-Net denoisers contain K blocks, let ϵ_{θ_i} be the i -th U-Net denoiser, and $\epsilon_{\theta_i}^{(j)}$ be its j -th block. For the timestep t , it transforms the input features $\mathbf{x}_t^{(j)}$ into the output feature by

$$\mathbf{y}_{t,i}^{(j)} = \epsilon_{\theta_i}^{(j)}(\mathbf{x}_t^{(j)}, \mathbf{c}, t). \quad (2)$$

Note that because of the same architecture of all ϵ_{θ_i} , $\mathbf{y}_{t,i}^{(j)}$ has the same shape, i.e., $\mathbf{y}_{t,i}^{(j)} \in \mathbb{R}^{h_j \times w_j \times c_j}$, where h_j , w_j , and c_j are the height, width, and channels, respectively. To achieve the output feature for the next block, a block $f_{\varphi}^{(j)}$ of

Algorithm 1 One forward process of Adaptive Feature Aggregation (AFA).

- 1: **Input:** Timestep t , Condition \mathbf{c} , Input latent \mathbf{x}_t , U-Net denoisers $\{\epsilon_{\theta_i}\}_{i=1}^N$, each of which contains K blocks, and SABW $f_\varphi^{(j)}$ for j -th U-Net block.
 - 2: **Output:** Predicted noise $\hat{\epsilon}_t$.
 - 3: Initialize an empty stack \mathcal{S} to store the features from the skip connections;
 - 4: $\mathbf{x}_t^{(1)} \leftarrow \mathbf{x}_t$;
 - 5: **for** block index j from 1 to K **do**
 - 6: \triangleright *Ensembling the j -th U-Net block by SABW feature aggregator $f_\varphi^{(j)}$*
 - 7: **for** U-Net denoiser index i from 1 to N **do**
 - 8: Get the output feature $\mathbf{y}_{t,i}^{(j)}$ base on Eq. (2);
 - 9: **end for**
 - 10: Get $\mathbf{y}_t^{(j)}$ by aggregating all $\mathbf{y}_{t,i}^{(j)}$ base on Eq. (3) for the next block;
 - 11: **if** $(j+1)$ -th block is down-sampling block **then**
 - 12: $\mathbf{x}_t^{(j+1)} \leftarrow \mathbf{y}_t^{(j)}$ and push $\mathbf{y}_t^{(j)}$ into \mathcal{S} ;
 - 13: **else if** $(j+1)$ -th block is up-sampling block **then**
 - 14: Pop \mathbf{y}_t^s from \mathcal{S} and $\mathbf{x}_t^{(j+1)} \leftarrow \text{concat}(\mathbf{y}_t^{(j)}, \mathbf{y}_t^s)$;
 - 15: **else**
 - 16: $\mathbf{x}_t^{(j+1)} \leftarrow \mathbf{y}_t^{(j)}$;
 - 17: **end if**
 - 18: **end for**
 - 19: $\hat{\epsilon}_t \leftarrow \mathbf{x}_t^{(K)}$;
 - 20: **return** predicted noise $\hat{\epsilon}_t$.
-

SABW is employed to aggregate $\{\mathbf{y}_{t,i}^{(j)}\}_{i=1}^N$,

$$\mathbf{y}_t^{(j)} = f_\varphi^{(j)}(\{\mathbf{y}_{t,i}^{(j)}\}_{i=1}^N, \mathbf{c}, t) \in \mathbb{R}^{h_j \times w_j \times c_j}, \quad (3)$$

where φ is the parameters of the SABW block. As a whole, the j -th ensembled block of these U-Net denoisers can be formulated as

$$\mathbf{y}_t^{(j)} = \mathcal{F}_\Theta^{(j)}(\mathbf{x}_t^{(j)}, \mathbf{c}, t), \quad (4)$$

where Θ is the parameter collection of φ and all the θ_i . It can be deduced that an ensembled block operates with the same functionality as a single block.

3.3 Spatial-Aware Block-Wise Feature Aggregator

The Spatial-Aware Block-Wise (SABW) feature aggregator is learned to aggregate output features of each block from multiple U-Net denoisers. We design SABW to learn spatial attention to reweight the contributions of these U-Net denoisers at each spatial position. Specifically, the spatial attention map $\mathbf{A}_t^{(j)}$ for N U-Net denoisers is achieved by

$$\mathbf{F}_t^{(j)} = g_\varphi^{(j)}(\{\mathbf{y}_{t,i}^{(j)}\}_{i=1}^N, \mathbf{c}, t) \in \mathbb{R}^{h_j \times w_j \times N}, \quad (5)$$

$$\mathbf{A}_t^{(j)} = \text{softmax}(\mathbf{F}_t^{(j)}) \in [0, 1]^{h_j \times w_j \times N}, \quad (6)$$

where, $\mathbf{F}_t^{(j)}$ is the output of the learnable network of SABW g_φ . Note that all the parameters of SABW (*i.e.*, φ) are used to learn spatial attention. The ensembled output feature is achieved by

$$\mathbf{y}_t^{(j)} = \mathcal{F}_\theta^{(j)}(\mathbf{x}_t^{(j)}, \mathbf{c}, t) = \sum_{i=1}^N \mathbf{A}_{t,i}^{(j)} \otimes \mathbf{y}_{t,i}^{(j)}, \quad (7)$$

where \otimes is the element-wise multiplication. $\mathbf{A}_{t,i}^{(j)} \in \mathbb{R}^{h_j \times w_j \times 1}$ is the spatial attention map for the i -th U-Net denoiser.

This spatial attention operation is based on an important experimental insight as shown in Fig. 1. The divergent denoising capabilities of multiple diffusion models will dynamically change in different spatial locations. Thus, better generation performance can be achieved by enabling multiple models to collaborate at different spatial locations.

Specifically, based on the denoising loss (*i.e.*, Eq. (1)), the denoising capability⁴ of ϵ_θ for $(\mathbf{x}_0, \mathbf{c})$ at timestep t can be defined as $-\mathbb{E}_{\epsilon \sim \mathcal{N}(\mathbf{0}, \mathbf{I})} \|\hat{\epsilon}_t - \epsilon\|^2$, where $\hat{\epsilon}_t = \epsilon_\theta(\mathbf{x}_t, \mathbf{c}, t)$. For the spatial location (x, y) , the denoising capability is formulated as $-\mathbb{E}_{\epsilon \sim \mathcal{N}(\mathbf{0}, \mathbf{I})} \|\hat{\epsilon}_{(x,y)} - \epsilon_{(x,y)}\|^2$, which considers the noise prediction errors at the spatial location (x, y) .

For example, as shown in Fig. 1, we employ three SD models to present their positional denoising capability on the specific image and textual prompt by Monte-Carlo sampled noises. We demonstrate the results of four patches which indicate that the divergent denoising capabilities of the three models vary at different spatial locations. SABW is learned to incorporate these denoisers to achieve stronger denoising capability at all spatial locations at the block level.

To implement g_φ in Eq. (5), SABW applies a ResNet [15] layer to introduce timesteps by adding the time embedding into the feature map, and a Transformer [54] layer to introduce textual prompts by the cross-attention,

$$\mathbf{Y}_t^{(j)} \leftarrow \text{concat}(\{\mathbf{y}_{t,i}^{(j)}\}_{i=1}^N) \in \mathbb{R}^{h_j \times w_j \times (N \cdot c_j)}, \quad (8)$$

$$\mathbf{H}_t^{(j)} \leftarrow \text{ResLayer}(\mathbf{Y}_t^{(j)} + \gamma(t)) \in \mathbb{R}^{h_j \times w_j \times d}, \quad (9)$$

$$\mathbf{O}_t^{(j)} \leftarrow \text{TransformerLayer}(\mathbf{H}_t^{(j)}, \mathbf{c}) \in \mathbb{R}^{h_j \times w_j \times d}, \quad (10)$$

$$\mathbf{F}_t^{(j)} \leftarrow \text{ZeroInitConv}(\mathbf{O}_t^{(j)}) \in \mathbb{R}^{h_j \times w_j \times N}, \quad (11)$$

where γ is used to map the timestep into the time embedding with the same shape of $\mathbf{Y}_t^{(j)}$. d is the hidden state dimension. $\text{ZeroInitConv}(\cdot)$ is the convolution layer initialized by zero, which leads to equal attention weights for all denoisers before training. We aspire for the model to commence training from a completely equitable state.

⁴ Compared with the denoising loss in Eq. (1), the denoising capability is defined by adding the negative sign, because of a negative correlation between the denoising capability and the denoising loss.

Table 1: Quantitative comparison between our AFA with the three base models in Group I (*i.e.*, ER, MMR, and RV) and the baseline methods.

	COCO 2017				Draw Bench Prompts			
	FID ↓	IS	CLIP-I	CLIP-T	AES	PS	HPSv2	IR
Base Model A	13.01	5.65	.6724	.2609	5.4102	21.6279	27.8007	.3544
Base Model B	13.45	5.43	.6775	.2652	5.5013	21.4624	27.7246	.2835
Base Model C	12.32	6.32	.6890	.2566	5.4881	21.8031	27.9652	.3922
Weighted Merging [56]	10.65	6.93	.6861	.2626	5.4815	21.7272	27.9086	.3909
MBW [33]	11.03	6.51	.6870	.2624	5.4812	21.7201	27.9080	.3922
autoMBW [4]	13.35	5.51	.6772	.2577	5.5056	21.4785	27.8192	.3672
MagicFusion [68]	10.53	6.85	.6751	.2620	5.3431	21.3840	27.8105	.3317
AFA (Ours)	9.76	7.14	.6926	.2675	5.5201	21.8263	27.9734	.4388

3.4 Training

Given the ensembled denoiser with AFA \mathcal{F}_Θ , the training object is the same as the denoising loss in Eq. (1),

$$\mathcal{L} = \mathbb{E}_{\mathbf{x}_0, \epsilon \sim \mathcal{N}(\mathbf{0}, \mathbf{I}), \mathbf{c}, t} \|\mathcal{F}_\Theta(\mathbf{x}_t, \mathbf{c}, t) - \epsilon\|^2. \quad (12)$$

Note that the parameters Θ contains both the parameters of SABW φ and the parameters of all U-Net denoisers $\{\theta_i\}_{i=1}^N$, where φ are learnable, and $\{\theta_i\}_{i=1}^N$ are frozen.

A well-trained AFA ensembles multiple U-Net denoisers to enhance the denoising capability in every block when experiencing different prompts, initial noises, denoising steps, and spatial locations. It leads to smaller denoising errors and stronger generation performance.

3.5 Inference

The inference of AFA starts from the sampled Gaussian noise. Then, the diffusion scheduler (*e.g.*, DDIM [51], PNDM [27], DPM-Solver [29, 30], *etc.*) is applied to generate images with multiple denoising steps.

For each inference step, the noise prediction relies on the technique of Classifier-Free Guidance (CFG) [18], which is formulated as

$$\hat{\epsilon}_t^{\text{pred}} = \hat{\epsilon}_t^{\text{uc}} + \beta_{\text{CFG}}(\hat{\epsilon}_t^{\text{c}} - \hat{\epsilon}_t^{\text{uc}}). \quad (13)$$

Among them, $\hat{\epsilon}_t^{\text{pred}}$, $\hat{\epsilon}_t^{\text{uc}}$, $\hat{\epsilon}_t^{\text{c}}$, and β_{CFG} are the final predicted noise, the predicted noise with condition, the predicted noise without condition, and a guidance scale, respectively. The latent for the next step is

$$\mathbf{x}_{t-1} = \frac{1}{\sqrt{\alpha_t}} \mathbf{x}_t - \frac{\sqrt{1-\alpha_t}}{\sqrt{\alpha_t}} \hat{\epsilon}_t^{\text{pred}}. \quad (14)$$

Finally, the generated image is achieved from the latent by a VAE decoder.

Table 2: Quantitative comparison between our AFA with the three base models in Group II (*i.e.*, AR, CR, and RCR) and the baseline methods.

	COCO 2017				Draw Bench Prompts			
	FID ↓	IS	CLIP-I	CLIP-T	AES	PS	HPSv2	IR
Base Model A	12.12	5.66	.6849	.2623	5.5641	21.8013	28.0183	.4238
Base Model B	12.41	5.59	.6818	.2580	5.5027	21.7249	28.0343	.4202
Base Model C	12.05	5.95	.6638	.2642	5.5712	21.4936	27.8089	.3367
Weighted Merging [56]	11.53	6.56	.6824	.2631	5.5756	21.7516	28.0014	.4387
MBW [33]	12.06	6.42	.6826	.2632	5.5772	21.7487	28.0029	.4396
autoMBW [4]	12.39	5.62	.6774	.2588	5.5478	21.5135	27.9873	.3513
MagicFusion [68]	11.63	7.13	.6790	.2640	5.4674	21.4270	27.9608	.4194
AFA (Ours)	10.27	7.42	.6855	.2717	5.5798	21.8059	28.0371	.4892

4 Experiments

4.1 Experiment Settings

Base Models. We select six popular models with the same architecture from SDv1.5 [49] in CivitAI. There are twelve down-sampling blocks, one middle block, and twelve up-sampling blocks for each model. These models are randomly divided into two groups, with three models in each group. The models from the same group will be ensembled.

- **Group I** contains EpicRealism (ER) [9], MajicMixRealistic (MMR) [31], and RealisticVision (RV) [42];
- **Group II** contains AbsoluteReality (AR) [1], CyberRealistic (CR) [6], and RealCartoonReslistic (RCR) [41].

Training. AdamW [28] is used as the optimizer with a learning rate of 0.0001 and a weight decay of 0.01. Note that only the parameters of SABW are optimized, while those of U-Net denoisers are frozen. Our AFA framework is trained on 10,000 samples from the dataset JourneyDB [37] for 10 epochs with batch size 8. To enable CFG, we use a probability of 0.1 to drop textual prompts.

Evaluation Protocols. For a fair comparison, all the methods generate 4 images by DDIM [17] for 50 inference steps. The CFG weight β_{CFG} in Eq. (13) is set to 7.5. We evaluate the models with two datasets, which are COCO 2017 [26] and Draw Bench Prompts [48], respectively.

- **COCO 2017** comprises 118,287 and 5,000 image-caption pairs in the test and validation sets. All the models generate images with a resolution of 256×256 . We apply four metrics to evaluate the generation performance, which are Fréchet Inception Distance (FID), Inception Score (IS), CLIP-I, and CLIP-T, respectively. FID and IS are applied to the test set, while CLIP-I and CLIP-T are applied to the validation set. Both FID and IS are metrics

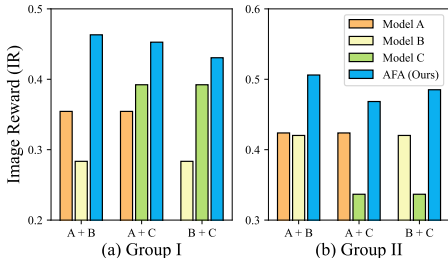


Fig. 3: Quantitative comparison between AFA with the two base models.

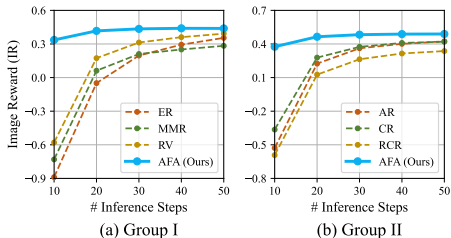


Fig. 4: Effect of varying inference steps.

to assess the quality of generated images. Note that lower FID means better quality. CLIP-I is the similarity between the CLIP [38] images embeddings of generated images and that of images from the image-caption pairs. CLIP-T is the CLIPScore [16] between the generated images with the captions.

- **Draw Bench Prompts** contains 200 evaluation prompts. All the models generate images with a resolution of 512×512 . We apply 4 evaluation metrics, which are AES [2], Pick Score (PS) [23], HPSv2 [59], and Image Reward (IR) [60], respectively. All three metrics evaluate the performance by a model that simulates human preferences. The evaluations are conducted 20 times to ensure statistical significance.

Baselines. We compare our AFA with several methods, including three merging-based methods (*i.e.*, Weighted Merging [56], MBW [33], and autoMBW [4]) and one ensembling-based method (*i.e.*, MagicFusion [68]). These baselines are also evaluated on two evaluation protocols under two model groups.

4.2 Quantitative Comparison

The results of the two evaluation protocols are summarized in Tab. 1 and Tab. 2. Generally, compared with base models, performance improvements are achieved by our AFA. For COCO 2017, after being ensembled by AFA, FID, IS, CLIP-I, and CLIP-T exhibit enhancements under both Group I and Group II. This indicates that the quality of our generated images is more closely with the dataset images. Additionally, the contexts of our generated images align more closely with those of the dataset images and corresponding captions. For Draw Bench Prompts, all four metrics show improvements under both Group I and Group II. The improvement on AES suggests that the aesthetics of our generated images surpass those generated by the base models. The improvements on PS, HPSv2, and IR suggest that the general generation capability can be boosted by applying AFA. Overall, the quantitative results validate the effectiveness of our AFA in ensembling text-to-image diffusion models.

While MagicFusion attains impressive performance in style-transferring and object-binding by ensembling two U-Net denoisers, it fails to achieve superior

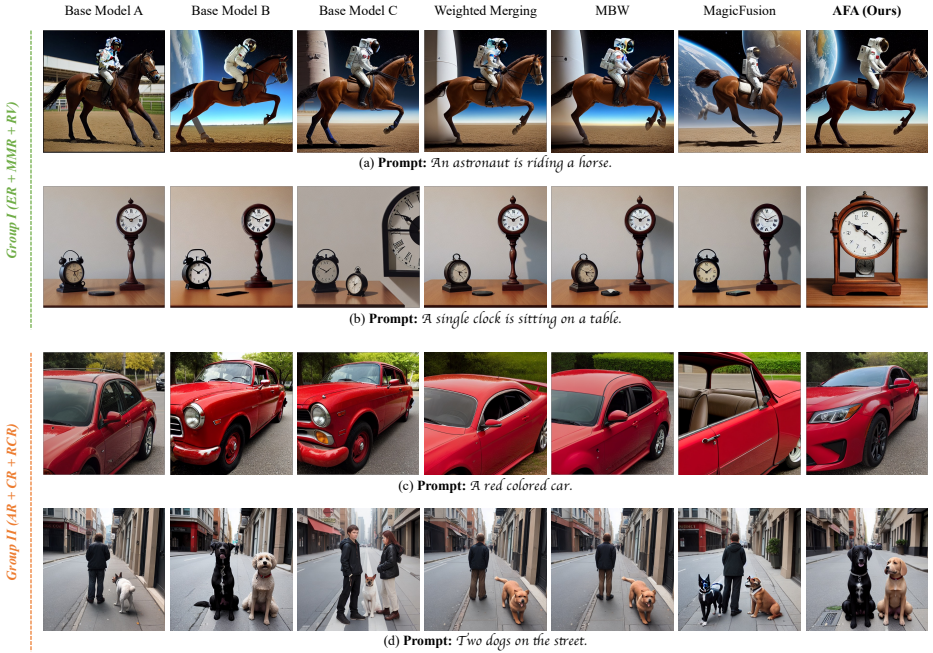


Fig. 5: Qualitative comparison between AFA with the base models and the baselines.

general generation when ensembling multiple U-Net denoisers. The merging-based methods, such as Weighted Merging, MBW, and autoMBW, do not always produce models with superior generation capabilities. For instance, under Group II, Weighted Merging achieves a better IR compared to the base models, but under Group I, it yields a lower IR. This could be attributed to the fixed contributions of merged models, which are determined by a set of predefined merging weights. Consequently, these methods fail to effectively facilitate collaboration between models to compensate for each other’s weaknesses and improve their generative capabilities. Compared with these baselines, our AFA consistently achieves better performance, demonstrating its superiority.

As depicted in Fig. 3, we use AFA to ensemble two models from Group I or Group II, and present the IR scores of base models and the ensembled models on Draw Bench Prompts. The results show that AFA significantly improves the performance when ensembling two U-Net denoisers. The results presented in Tab. 1, Tab. 2, and Fig. 3 indicate that AFA can be effectively applied to various model combinations and can be extended to accommodate different numbers of models. Simultaneously, it consistently achieves superior generation performance compared to a single base model.

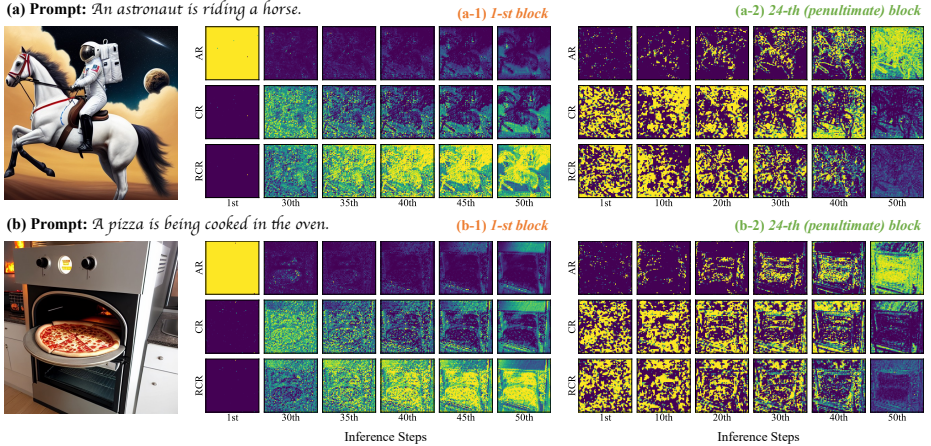


Fig. 6: Visualization of the learned attention maps. In each attention map, the position with a lighter color means a higher attention weight. Conversely, the position with a darker color means a lower attention weight.

4.3 Qualitative Comparison

As shown in Fig. 5, we present a qualitative comparison of the results from the base models, some of the baseline methods, and our AFA, which allows us to make several insightful observations. Firstly, AFA can generate images with better aesthetics. For example, in Fig. 5 (a) and (c), AFA can generate images with improved composition and finer details, compared to both the base models and the baseline methods. Secondly, AFA excels in achieving superior context alignment. For example, in Fig. 5 (b), all the base models and the baseline methods generate images containing more than *one clock*, despite the textual prompt specifying *a single clock*. In contrast, only our AFA generates the image with just one clock, accurately reflecting the provided context. Thirdly, AFA can focus on the correct context of the base models and drop out the incorrect context. For example, in Fig. 5 (d), only the base model B generates the image with *two dogs*, while the baseline methods do not fully trust the base model B, and generate the images with *people*. Only our AFA fully trusts the base model B, and generates the image with *two dogs*, which aligns with the textual context.

4.4 Model Study

Visualization of Attention Maps. As shown in Fig. 6, we select to visualize the attention maps of the first and the penultimate (*i.e.*, 24-th) blocks, both of which are learned by ensembling models in Group II through our AFA. For the first block, the learned attention maps seem to concentrate solely on the feature map of AR at the first inference stage. However, at the last few inference steps (*i.e.*, from the 30th to the 50th step), the roles of the feature maps from different models begin to diverge. The attention maps tend to highlight the contextual

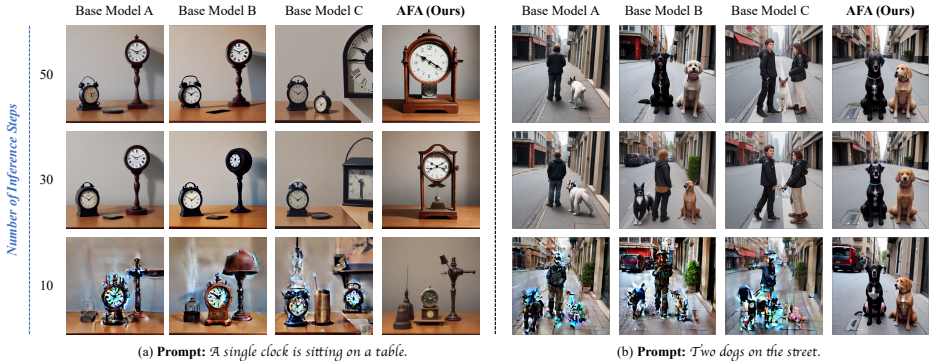


Fig. 7: Qualitative comparison under different inference steps.

body (*i.e.*, the *astronaut* and the *horse* in Fig. 6 (a), and the *pizza* and the *oven* in Fig. 6 (b)) in the feature map of RCR, while focusing on the background elements in the feature maps of AR and CR. For the penultimate block, as the inference progresses, the learned attention maps gradually emphasize the contextual body within the feature map of AR, while concentrating on the background within the feature maps of both CR and RCR. Overall, the visualization of the learned attention maps indicates that our AFA can effectively ensemble diffusion models based on the context and the timesteps.

Effect of Fewer Inference Steps. As shown in Fig. 4 and Fig. 7, we investigate the resilience of our AFA to a reduction in the inference steps. Fig. 4 clearly shows a significant drop in the performance of the base models when the number of inference steps is reduced. However, the performance of our AFA remains almost stable when the number of inference steps is reduced from 50 to 20, and only experiences a slight decline when the number of inference steps is reduced to 10. Additionally, in Fig. 7, we can find that the quality of the images generated by the base models deteriorates with the reduction of inference steps. In contrast, our AFA stably generates high-quality images. Overall, it indicates that greater tolerance for fewer inference steps will be achieved after ensembling by AFA. Furthermore, while a single inference step may require a proportional increase in time, the total time consumed by the entire inference process does not escalate in the same manner.

Ablation Study. As shown in Tab. 3, we conduct the ablation study to investigate the necessity of each component within our AFA. Firstly, we conduct experiments with the following settings. (1) **Only Ensembling Last Block:** The AFA ensembles only the last block, leaving all other blocks unaltered. (2) **Block-Wise Averaging:** Each block is ensembled by averaging the output feature maps, rather than using SABW. (3) **Noise Averaging:** Only the last block is ensembled by averaging the output feature maps (*i.e.*, predicted noises). The

observed performance declines in these settings suggest that the design of the AFA effectively contributes to the ensembling of diffusion models, thereby leading to improved generation. Next, we conduct an ablation study on the spatial location from AFA, which learn only a single attention score (*i.e.*, a scalar) for the feature of each U-Net denoiser, as opposed to an attention map. The observed decrease in performance suggests that learning a spatial attention map to adaptively adjust the weights of various U-Net denoisers in the level of spatial location is beneficial for the ensemble of different diffusion models. Finally, we individually ablate the timestep and the textual condition which are introduced to AFA. The decreasing performance indicates that both the introduced timestep and textual condition play crucial roles in ensembling diffusion models by AFA.

Discussion on Computational Efficiency. (1) **Ensembling Methods.** Compared with another ensembling method (*i.e.*, MagicFusion), the computational efficiency of our AFA for a single inference step aligns closely with it. Both AFA and MagicFusion necessitate running all base models in one inference step. Although SABW in AFA introduces additional parameters, which leads to more computations, it has fewer than the base models (about 1/16). To be precise, our AFA may be marginally less efficient than MagicFusion on single inference steps, but the difference is practically negligible. (2) **Merging Methods.** Because the various models are collapsed into one model, the computational efficiency of the merging methods equals that of a single base model. For the base models and the merging methods, a single image generation takes about 7 seconds with 50 inference steps. When ensembling three such base models, a single generation will take about 22 seconds with the same inference steps. Compared with ensembling, the computation efficiency of one inference step of the merging methods is significantly higher. However, as we discussed in *Effect of Fewer Inference Steps* of Sec. 4.4, AFA shows remarkable tolerance for fewer inference steps. When limited to 20 inference steps, the performance of AFA does not significantly decline (as shown in Fig. 4), while the time consumed is reduced to about 8.8 seconds. This suggests that AFA has comparable computational efficiency with that of the base models or the merging methods throughout the entire inference process.

5 Conclusion

In this paper, we aim to ensemble multiple diffusion models to achieve better generation performance. To this end, we propose the Adaptive Feature Aggregation (AFA) method, which dynamically adjusts the contributions of multiple models at the feature level according to different prompts, initial noises, denoising steps, and spatial locations. Specifically, we design a lightweight Spatial-Aware Block-Wise feature aggregator that produces attention maps to adaptively aggregate the block-level intermediate features from multiple U-Net denoisers. Both the quantitative and qualitative experiments demonstrate that AFA achieves improvements in image quality and context alignment.

Table 3: Ablation study of AFA.

	IR (Group I)	IR (Group II)
AFA (Full Model)	.4388	.4892
Only Ensembling Last Block	.4176	.4374
Block-Wise Averaging	.4001	.4372
Noise Averaging	.3919	.4355
w/o Spatial Location	.4044	.4610
w/o Timestep	.4235	.4622
w/o Textual Condition	.4163	.4559

Limitation. A significant limitation of our AFA is that a single inference step may necessitate a proportional increase in inference time, resulting in lower computational efficiency for that step. Fortunately, due to its high tolerance for fewer inference steps, the total time consumed by the entire inference process does not escalate in the same manner. This results in a computational efficiency that is on par with that of the base models or the merging methods.

References

1. AbsoluteReality: <https://civitai.com/models/81458?modelVersionId=1085769>
2. AES: <https://laion.ai/blog/laion-aesthetics/> 10
3. Ainsworth, S.K., Hayase, J., Srinivasa, S.: Git re-basin: Merging models modulo permutation symmetries. arXiv preprint arXiv:2209.04836 (2022) 3
4. autoMBW: <https://github.com/Xerxemi/sdweb-auto-MBW> 2, 4, 8, 9, 10
5. Balaji, Y., Nah, S., Huang, X., Vahdat, A., Song, J., Kreis, K., Aittala, M., Aila, T., Laine, S., Catanzaro, B., et al.: ediffi: Text-to-image diffusion models with an ensemble of expert denoisers. arXiv preprint arXiv:2211.01324 (2022) 1, 3
6. CyberRealistic: <https://civitai.com/models/15003?modelVersionId=896809>
7. Ding, M., Yang, Z., Hong, W., Zheng, W., Zhou, C., Yin, D., Lin, J., Zou, X., Shao, Z., Yang, H., et al.: Cogview: Mastering text-to-image generation via transformers. NeurIPS (2021) 3
8. Don-Yehiya, S., Venezian, E., Raffel, C., Slonim, N., Katz, Y., Choshen, L.: Cold fusion: Collaborative descent for distributed multitask finetuning. arXiv preprint arXiv:2212.01378 (2022) 3
9. EpicRealism: <https://civitai.com/models/25694?modelVersionId=1340659>
10. Feng, Z., Zhang, Z., Yu, X., Fang, Y., Li, L., Chen, X., Lu, Y., Liu, J., Yin, W., Feng, S., et al.: Ernie-vilg 2.0: Improving text-to-image diffusion model with knowledge-enhanced mixture-of-denoising-experts. In: CVPR (2023) 1, 3
11. Frankle, J., Dziugaite, G.K., Roy, D., Carbin, M.: Linear mode connectivity and the lottery ticket hypothesis. In: International Conference on Machine Learning. pp. 3259–3269. PMLR (2020) 3
12. Freund, Y., Schapire, R.E.: A decision-theoretic generalization of on-line learning and an application to boosting. In: European conference on computational learning theory. pp. 23–37. Springer (1995) 2
13. Gafni, O., Polyak, A., Ashual, O., Sheynin, S., Parikh, D., Taigman, Y.: Make-a-scene: Scene-based text-to-image generation with human priors. In: ECCV (2022) 3

14. Goodfellow, I., Pouget-Abadie, J., Mirza, M., Xu, B., Warde-Farley, D., Ozair, S., Courville, A., Bengio, Y.: Generative adversarial nets. *NeurIPS* (2014) **3, 4**
15. He, K., Zhang, X., Ren, S., Sun, J.: Deep residual learning for image recognition. In: *CVPR* (2016) **5, 7**
16. Hessel, J., Holtzman, A., Forbes, M., Le Bras, R., Choi, Y.: Clipscore: A reference-free evaluation metric for image captioning. In: *Proceedings of the 2021 Conference on Empirical Methods in Natural Language Processing*. pp. 7514–7528 (2021) **10**
17. Ho, J., Jain, A., Abbeel, P.: Denoising diffusion probabilistic models. *NeurIPS* (2020) **1, 3, 4, 9**
18. Ho, J., Salimans, T.: Classifier-free diffusion guidance. *arXiv preprint arXiv:2207.12598* (2022) **8**
19. Ilharco, G., Ribeiro, M.T., Wortsman, M., Gururangan, S., Schmidt, L., Hajishirzi, H., Farhadi, A.: Editing models with task arithmetic. *arXiv preprint arXiv:2212.04089* (2022) **3**
20. Ilharco, G., Wortsman, M., Gadre, S.Y., Song, S., Hajishirzi, H., Kornblith, S., Farhadi, A., Schmidt, L.: Patching open-vocabulary models by interpolating weights. *NeurIPS* (2022) **3**
21. Jin, X., Ren, X., Preotiuc-Pietro, D., Cheng, P.: Dataless knowledge fusion by merging weights of language models. *arXiv preprint arXiv:2212.09849* (2022) **3**
22. Kingma, D.P., Welling, M.: Auto-encoding variational bayes. *arXiv preprint arXiv:1312.6114* (2013) **5**
23. Kirstain, Y., Polyak, A., Singer, U., Matiana, S., Penna, J., Levy, O.: Pick-a-pic: An open dataset of user preferences for text-to-image generation. *arXiv preprint arXiv:2305.01569* (2023) **10**
24. Kumari, N., Zhang, R., Shechtman, E., Zhu, J.Y.: Ensembling off-the-shelf models for gan training. In: *CVPR* (2022) **4**
25. Li, M., Gururangan, S., Dettmers, T., Lewis, M., Althoff, T., Smith, N.A., Zettlemoyer, L.: Branch-train-merge: Embarrassingly parallel training of expert language models. *arXiv preprint arXiv:2208.03306* (2022) **3**
26. Lin, T.Y., Maire, M., Belongie, S., Hays, J., Perona, P., Ramanan, D., Dollár, P., Zitnick, C.L.: Microsoft coco: Common objects in context. In: *ECCV* (2014) **9**
27. Liu, L., Ren, Y., Lin, Z., Zhao, Z.: Pseudo numerical methods for diffusion models on manifolds. *arXiv preprint arXiv:2202.09778* (2022) **8**
28. Loshchilov, I., Hutter, F.: Decoupled weight decay regularization. *arXiv preprint arXiv:1711.05101* (2017) **9**
29. Lu, C., Zhou, Y., Bao, F., Chen, J., Li, C., Zhu, J.: Dpm-solver: A fast ode solver for diffusion probabilistic model sampling in around 10 steps. *NeurIPS* (2022) **8**
30. Lu, C., Zhou, Y., Bao, F., Chen, J., Li, C., Zhu, J.: Dpm-solver++: Fast solver for guided sampling of diffusion probabilistic models. *arXiv preprint arXiv:2211.01095* (2022) **8**
31. MajicMixRealistic: <https://civitai.com/models/43331?modelVersionId=176425> **9**
32. Matena, M.S., Raffel, C.A.: Merging models with fisher-weighted averaging. *NeurIPS* (2022) **3**
33. MBW: <https://github.com/bbc-mc/sdweb-merge-block-weighted-gui> **2, 4, 8, 9, 10**
34. Mendes-Moreira, J., Soares, C., Jorge, A.M., Sousa, J.F.D.: Ensemble approaches for regression: A survey. *Acm computing surveys (csur)* **45**(1), 1–40 (2012) **4**

35. Nichol, A., Dhariwal, P., Ramesh, A., Shyam, P., Mishkin, P., McGrew, B., Sutskever, I., Chen, M.: Glide: Towards photorealistic image generation and editing with text-guided diffusion models. arXiv preprint arXiv:2112.10741 (2021) **1, 3**
36. Ortiz-Jimenez, G., Favero, A., Frossard, P.: Task arithmetic in the tangent space: Improved editing of pre-trained models. arXiv preprint arXiv:2305.12827 (2023) **3**
37. Pan, J., Sun, K., Ge, Y., Li, H., Duan, H., Wu, X., Zhang, R., Zhou, A., Qin, Z., Wang, Y., et al.: Journeydb: A benchmark for generative image understanding. arXiv preprint arXiv:2307.00716 (2023) **9**
38. Radford, A., Kim, J.W., Hallacy, C., Ramesh, A., Goh, G., Agarwal, S., Sastry, G., Askell, A., Mishkin, P., Clark, J., et al.: Learning transferable visual models from natural language supervision. In: International conference on machine learning. pp. 8748–8763. PMLR (2021) **10**
39. Ramesh, A., Dhariwal, P., Nichol, A., Chu, C., Chen, M.: Hierarchical text-conditional image generation with clip latents. arXiv preprint arXiv:2204.06125 **1(2), 3** (2022) **1, 3**
40. Ramesh, A., Pavlov, M., Goh, G., Gray, S., Voss, C., Radford, A., Chen, M., Sutskever, I.: Zero-shot text-to-image generation. In: International Conference on Machine Learning. pp. 8821–8831. PMLR (2021) **3**
41. RealCartoonReslistic: <https://civitai.com/models/97744?modelVersionId=104496> **9**
42. RealisticVision: <https://civitai.com/models/4201?modelVersionId=130072> **9**
43. Ren, Y., Suganthan, P., Srikanth, N.: Ensemble methods for wind and solar power forecasting—a state-of-the-art review. Renewable and Sustainable Energy Reviews **50**, 82–91 (2015) **4**
44. Rezende, D.J., Mohamed, S., Wierstra, D.: Stochastic backpropagation and approximate inference in deep generative models. In: International conference on machine learning. pp. 1278–1286. PMLR (2014) **5**
45. Rokach, L.: Ensemble-based classifiers. Artificial intelligence review **33**, 1–39 (2010) **4**
46. Rombach, R., Blattmann, A., Lorenz, D., Esser, P., Ommer, B.: High-resolution image synthesis with latent diffusion models. In: CVPR (2022) **1, 2, 3**
47. Ronneberger, O., Fischer, P., Brox, T.: U-net: Convolutional networks for biomedical image segmentation. In: Medical Image Computing and Computer-Assisted Intervention–MICCAI 2015: 18th International Conference, Munich, Germany, October 5–9, 2015, Proceedings, Part III 18. pp. 234–241. Springer (2015) **4, 5**
48. Saharia, C., Chan, W., Saxena, S., Li, L., Whang, J., Denton, E.L., Ghasemipour, K., Gontijo Lopes, R., Karagol Ayan, B., Salimans, T., et al.: Photorealistic text-to-image diffusion models with deep language understanding. NeurIPS (2022) **1, 3, 9**
49. SDv1.5: <https://huggingface.co/runwayml/stable-diffusion-v1-5> **9**
50. Sohl-Dickstein, J., Weiss, E., Maheswaranathan, N., Ganguli, S.: Deep unsupervised learning using nonequilibrium thermodynamics. In: International conference on machine learning. pp. 2256–2265. PMLR (2015) **1, 3, 4**
51. Song, J., Meng, C., Ermon, S.: Denoising diffusion implicit models. In: ICLR (2020) **8**
52. Stoica, G., Bolya, D., Bjorner, J., Hearn, T., Hoffman, J.: Zipit! merging models from different tasks without training. arXiv preprint arXiv:2305.03053 (2023) **3**
53. Tao, M., Tang, H., Wu, F., Jing, X.Y., Bao, B.K., Xu, C.: Df-gan: A simple and effective baseline for text-to-image synthesis. In: CVPR (2022) **3**

54. Vaswani, A., Shazeer, N., Parmar, N., Uszkoreit, J., Jones, L., Gomez, A.N., Kaiser, Ł., Polosukhin, I.: Attention is all you need. *NeurIPS* (2017) **3, 5, 7**
55. Vega-Pons, S., Ruiz-Shulcloper, J.: A survey of clustering ensemble algorithms. *International Journal of Pattern Recognition and Artificial Intelligence* **25**(03), 337–372 (2011) **4**
56. Weighted-Merging: <https://github.com/hako-mikan/sd-webui-supermerger> **2, 4, 8, 9, 10**
57. Wortsman, M., Ilharco, G., Gadre, S.Y., Roelofs, R., Gontijo-Lopes, R., Morcos, A.S., Namkoong, H., Farhadi, A., Carmon, Y., Kornblith, S., et al.: Model soups: averaging weights of multiple fine-tuned models improves accuracy without increasing inference time. In: *International Conference on Machine Learning*. pp. 23965–23998. PMLR (2022) **3**
58. Wortsman, M., Ilharco, G., Kim, J.W., Li, M., Kornblith, S., Roelofs, R., Lopes, R.G., Hajishirzi, H., Farhadi, A., Namkoong, H., et al.: Robust fine-tuning of zero-shot models. In: *CVPR* (2022) **3**
59. Wu, X., Hao, Y., Sun, K., Chen, Y., Zhu, F., Zhao, R., Li, H.: Human preference score v2: A solid benchmark for evaluating human preferences of text-to-image synthesis. *arXiv preprint arXiv:2306.09341* (2023) **10**
60. Xu, J., Liu, X., Wu, Y., Tong, Y., Li, Q., Ding, M., Tang, J., Dong, Y.: Imagereward: Learning and evaluating human preferences for text-to-image generation. *arXiv preprint arXiv:2304.05977* (2023) **10**
61. Xu, T., Zhang, P., Huang, Q., Zhang, H., Gan, Z., Huang, X., He, X.: Attngan: Fine-grained text to image generation with attentional generative adversarial networks. In: *CVPR* (2018) **3**
62. Xue, Z., Song, G., Guo, Q., Liu, B., Zong, Z., Liu, Y., Luo, P.: Raphael: Text-to-image generation via large mixture of diffusion paths. *arXiv preprint arXiv:2305.18295* (2023) **1, 3**
63. Yang, P., Hwa Yang, Y., B Zhou, B., Y Zomaya, A.: A review of ensemble methods in bioinformatics. *Current Bioinformatics* **5**(4), 296–308 (2010) **4**
64. Yu, J., Xu, Y., Koh, J.Y., Luong, T., Baid, G., Wang, Z., Vasudevan, V., Ku, A., Yang, Y., Ayan, B.K., et al.: Scaling autoregressive models for content-rich text-to-image generation. *arXiv preprint arXiv:2206.10789* (2022) **3**
65. Zhang, H., Koh, J.Y., Baldrige, J., Lee, H., Yang, Y.: Cross-modal contrastive learning for text-to-image generation. In: *CVPR* (2021) **3**
66. Zhang, H., Yin, W., Fang, Y., Li, L., Duan, B., Wu, Z., Sun, Y., Tian, H., Wu, H., Wang, H.: Ernie-vilg: Unified generative pre-training for bidirectional vision-language generation. *arXiv preprint arXiv:2112.15283* (2021) **3**
67. Zhang, J., Chen, S., Liu, J., He, J.: Composing parameter-efficient modules with arithmetic operations. *arXiv preprint arXiv:2306.14870* (2023) **3**
68. Zhao, J., Zheng, H., Wang, C., Lan, L., Yang, W.: Magicfusion: Boosting text-to-image generation performance by fusing diffusion models. *arXiv preprint arXiv:2303.13126* (2023) **4, 8, 9, 10**
69. Zhao, Y., Gao, J., Yang, X.: A survey of neural network ensembles. In: *2005 international conference on neural networks and brain*. vol. 1, pp. 438–442. IEEE (2005) **4**
70. Zhou, Z.H.: *Ensemble methods: foundations and algorithms*. CRC press (2012) **4**
71. Zhu, M., Pan, P., Chen, W., Yang, Y.: Dm-gan: Dynamic memory generative adversarial networks for text-to-image synthesis. In: *CVPR* (2019) **3**